[GRI] (#750)

Study of water Cherenkov detector to determine air shower arrival directions with accuracy

A. Shiomi,[a] H. Nakada,[b] Y. Katayose,[b] M. Ohnishi,[c] T.K. Sako[c] and K. Hibino[d]

[a] College of Industrial Technology, Nihon University, Japan, [b] Faculty of Engineering, Yokohama National University, Japan,
[c] Institute for Cosmic Ray Research, University of Tokyo, Japan, [d] Faculty of Engineering, Kanagawa University, Japan

ICRC2021
37th International Cosmic Ray Conference

The Astroparticle Physics Conference
12 – 23 July 2021
Berlin, Germany

Motivation

Several spread TeV gamma-ray sources have been observed in the galaxy by several experimental groups. Experiments with high angular resolution that can detect gamma rays in the 100 TeV region will help study acceleration mechanisms of those gamma-ray sources. In recent years, three groups using extensive air shower arrays have reported detecting gamma rays in the 100 TeV region from astronomical objects in the galaxy. In extensive air shower experiments, an arrival direction of a cosmic ray is determined by estimating a shape of a front surface of an air shower based on a detected secondary particle density distribution and detection time. The density of secondary gamma rays of an air shower is several times that of secondary electrons and positrons in an air shower and the difference increases as the distance from the shower axis increases. Therefore, secondary gamma-ray measurements are key to determining the arrival direction of the shower. We report the results of investigating the effect of secondary gamma rays on the time determination accuracy of an air shower front using a Monte Carlo simulation. We also report the results of examining different detector structures to improve the time resolution using a water Cherenkov detector, which has high detection efficiency for secondary gamma rays.

Simulation (1)

Characteristics of the electromagnetic component of the induced air shower front

Table1. Gamma-ray air shower produced to investigate the properties of secondary particles by CORSIKA 7.6400 code.

Primary energy	500 TeV	H.E. model	QGSJET-II-04
Induced zenith	0°	L.E. model	FLUKA
Altitude	4,740 m	Number of events	1,000

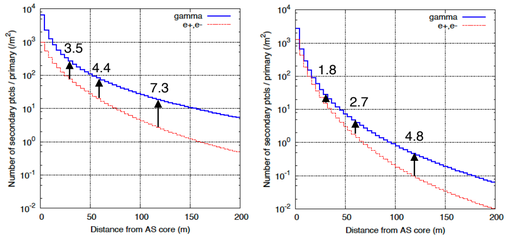

(a) 1MeV < E < 100 MeV

(b) E ≧ 100 MeV

Fig. 1. Lateral distribution of secondary gamma rays and electron-positrons by 500 TeV primary gamma rays.

Secondary gamma rays become more predominant as the distance from the center of the shower increases. It can be seen that there are more secondary gamma rays than secondary electrons, even for particles with energies greater than the critical energy of electrons.

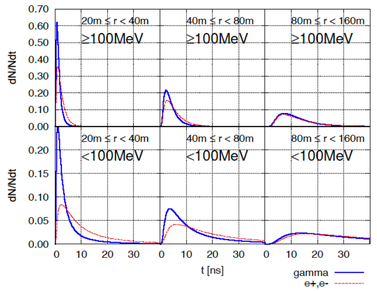

Fig. 2. Arrival time distribution of secondary particles with respect to the distance from the shower core. The vertical axis represents the frequency per unit time, and the area is normalized.

The distribution of secondary gamma rays became slightly sharper than secondary electrons, and secondary gamma rays tended to be concentrated in the front. The difference between the distribution of secondary gamma rays and electrons is small near 120 m from the center of the shower core, however, the density of secondary gamma rays is several times higher than that of electrons.

Reference

[1] M. Amenomori, et al., Potential PeVatron supernova remnant G106.3+2.7 seen in the highest-energy gamma rays, Nature Astronomy (2021). https://DOI.org/10.1038/s41550-020-01294-9
[2] M. Amenomori, et al., Development and performance test of a prototype air shower array for search for gamma ray point sources in the very high energy region, NIM A, 288, 619 (1990)
[3] J. Poirier, S. Mikochi, Improving the angular resolution of existing air shower arrays by adding a thin layer of lead, NIM A, 257, 473 (1987)
[4] D. Heck et al., CORSIKA: A Monte Carlo ode to Simulate Extensive Air Showers, Report FZKA, 6019, Forschungszentrum Karlsruhe (1998)
[5] S. Agostinelli, et al. GEANT4 - a simulation toolkit, Nucl. Instrum. Methods Phys. Res. A, 506 250 (2003)
[6] J. Nishimura and K. Kamata, The Lateral and the Angular Structure Functions of Electron Shower, Progr. Theor. Phys. Suppl., 6,93 (1958)
[7] A. Shiomi, et al., Study of Performance Improvement for Air Shower Array with Surface Water Cherenkov Detectors, 35th International Cosmic Ray Conference (Busan, Korea 2017), PoS(ICRC2017)380

Acknowledgements

This work was supported by JSPS KAKENHI Grant Number JP15K05108.

Simulation (2)

Verification of the effect of secondary gamma rays on direction determination

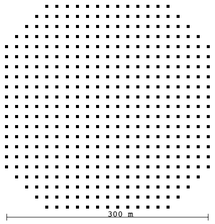

Fig.3. Schematic view of the AS arrays. Black squares are the positions of the normal or virtual plastic scintillation detectors.

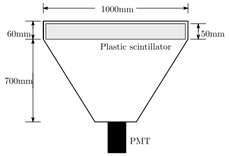

Fig.4. Schematic view of the scintillation detector.

Compare an array of standard plastic scintillation detectors with an array of virtual plastic scintillation detectors that can replace gamma rays with electrons

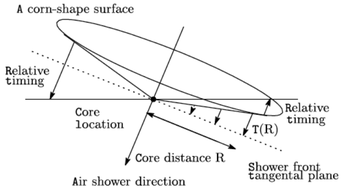

Fig.5. Description of cone-shape fitting to air-shower front. The slope of the cone is defined as a function of the distance from the obtained core location $R_{(m)}$ as $T(R_i) = R_i (\tan \psi)/c$.

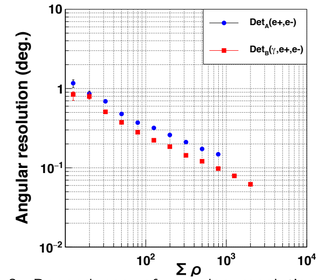

Fig.6. Dependence of angular resolution on the number of detected particles. The horizontal and vertical axis, respectively, represent the number of detected particles and angular resolution, which is the result of a primary gamma ray of 500 TeV (Table 1). The wide range of the horizontal axis ($\Sigma \rho$) is achieved by removing the secondary particles produced by each primary particles by a fixed percentage from 0 to 99%.

Not only does the angular resolution decrease in inverse proportion to the square root of the number of measured particles, but if the total number of measured particles is the same, secondary gamma rays contribute to better angular resolution than electrons. When secondary gamma rays could be measured with electron-like sensitivity, a shower of 500 TeV showed an improvement in angle resolution of about 40%.

Simulation (3)

Optimal water Cherenkov detector design for measuring air shower fronts

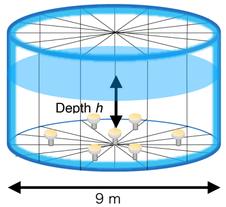

Fig.7. Schematic view of a WCD. WCD is made by 3.0 mm-thick stainless steel water tank of 9.0 m diameter. Upward-facing 8" PMTs are installed on the floor. The light reflectance of the inner wall of the tank is 0 %.

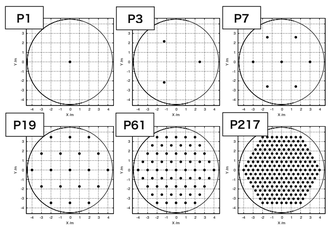

Fig. 8. Arrangement of PMTs used in the simulation. PMTs were placed at equal intervals in a circle with a radius of 4.5 m. The performance of the WCD was evaluated in six cases. When the number of PMTs is i, a label of "Pi" is applied.

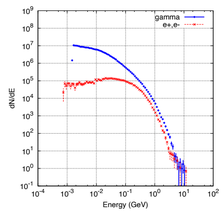

Fig.9. Energy distribution of shower particles used in WCD response calculation. Among the fastest (within 1 ns) secondary particles of 10 TeV gamma rays, only events 30 m away from the shower core was used.

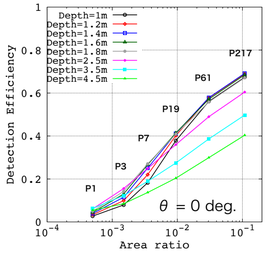

Fig. 10. Dependence of detection efficiency on PMT sensitivity area. The horizontal axis represents the ratio of the PMT sensitivity area to the tank area. Trigger condition is any one of PMTs (≧ 3 p.e.) in any WCD.

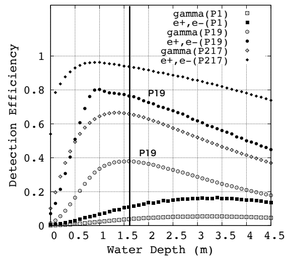

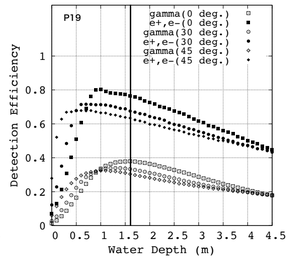

Fig.11. Dependence of detection efficiency on water depth. The left shows the results for electrons and gamma rays at an incident angle of 0 degree. The detection efficiency is plotted for P1, P19, and P217. The right shows the water depth dependency of the detection efficiency in the case of P19. The detection efficiencies of electrons and gamma-rays are plotted for incident particle angles of 0◦, 30◦, and 45◦.

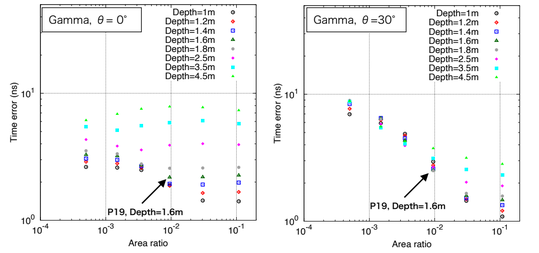

Fig. 12. Dependence of time error between ceiling of the WCD and one of the first detected PMT on PMT sensitivity area for gamma rays incident at 0° and 30°.

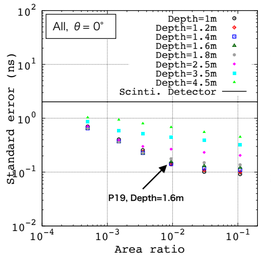

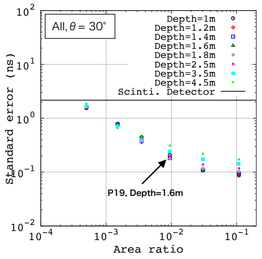

Fig. 13. Dependence of standard error of detection time on PMT sensitivity area for particles incident at 0° and 30°.

Using 19 PMTs with a diameter of 8 inches in a detector installed in a water tank with a radius of 4.5 m and a depth of 1.6 m, detection efficiencies of about 0.38 and 0.76 were obtained for vertically incident gamma rays and electrons, respectively. The detection time error of secondary gamma rays was about 2.18 ns at an incident angle of 0 °.